Lattice Boltzmann simulations of the acoustic radiation from waveguides



2007 J. Phys. A: Math. Theor. 40 397

(http://iopscience.iop.org/1751-8121/40/3/004)

INSTITUTE OF PHYSICS PUBLISHING JOURNAL OF PHYSICS A: MATHEMATICAL AND THEORETICAL

J. Phys. A: Math. Theor. **40** (2007) 397–408 doi:10.1088/1751-8113/40/3/004

# Lattice Boltzmann simulations of the acoustic radiation from waveguides

**A R da Silva and G P Scavone**

Computational Acoustic Modeling Laboratory, McGill University, 555 Sherbrooke Street West, Montreal, Quebec, CA H3A 1E3, Canada

E-mail: andrey.dasilva@mail.mcgill.ca

Received 25 July 2006, in final form 6 November 2006
Published 20 December 2006
Online at stacks.iop.org/JPhysA/40/397

**Abstract**

The application of the lattice Boltzmann method to evaluate the far-field normal mode radiation pattern from an unflanged cylindrical waveguide is considered in this paper. The parameters associated with the radiation process such as directivity factor, end correction and reflection coefficient are predicted and compared with the theory of inviscid normal mode radiation derived by Levine and Schwinger. The good agreement found between numerical and analytical results, as well as the ability to intrinsically resolve fluid dynamics and acoustics problems suggests that the lattice Boltzmann approach is a useful tool to predict complex phenomena involving duct acoustics, such as nonlinear dissipation and the interaction between the acoustic field and the presence of a mean flow.

PACS numbers: 43.55.Rg, 47.35.Rs, 43.20.+g

## 1. Introduction

Much attention has been focused over the last century on the mechanisms of acoustic radiation from open-ended waveguides. Analytical predictions of the generated external sound field are usually derived based on a common simplification in which the sharp edge at the open end is substituted by a surrounding infinite flange. This unrealistic boundary condition can be useful for predicting the radiation within the hemisphere beyond the open end but becomes inaccurate for the prediction of backward radiation, as demonstrated experimentally by Tyler and Sofrin (1962). This is due to the fact that the infinite flange approach neglects the influence of diffraction effects that take place at the sharp edge of a realistic open end.

The characteristics of the external sound field can be determined from the reflection experienced by the outgoing wave at the open end of the waveguide. This reflection is a function of the wavelength $\lambda$ and will be determined by the boundary condition at that point. The reflection also acts to increase the effective length of the waveguide by a certain fraction of its output radius $a$ (Pierce 1981). Several analytical predictions for the reflection coefficient

  

$R$, as well as for the end correction $l$, have been proposed over the years for normal mode propagation (plane waves). Rayleigh (1877) found $l \simeq 0.6a$ for an unflanged cylinder in the low-frequency limit ($ka \ll 1$, where $k = 2\pi/\lambda$ is the wavenumber). Many years later, King (1936) presented the exact solution for $l$ of a flanged cylinder. At low frequencies he found $l = 0.82a$. Levine and Schwinger (1948) were the first to obtain an exact solution for $l$ of an unflanged cylinder by using the Wiener–Hopf technique. In the low-frequency limit, they found $l = 0.6133a$. Furthermore, they also presented exact expressions for $R$ and for the far-field acoustic pressure directivity $G_\phi$ around the cylinder's open end, both as functions of the characteristic parameter $ka$. However, predicting the acoustic field with the analytical approach becomes increasingly difficult as one considers waveguides with complex geometries, high modes of propagation or even nonlinearities caused by the interaction between mean flow and the acoustic field, such as vortex shedding (Powell 1964, Schlichting 2004) and energy losses (Howe 1984). In this case, numerical techniques are more likely to be suitable.

Most numerical techniques resolve the problem of wave radiation from a waveguide using continuum theory, where the sound field is described by temporal and spatial evolutions of the acoustic domain through partial differential equations. As examples, Chen *et al* (2004) recently predicted the far-field normal mode radiation from an unflanged cylinder using a computational aeroacoustics (CAA) technique involving the linearized and integral solutions of Euler and Ffowcs-Williams–Hawkings equations (Williams and Hawkings 1969), respectively. The same problem was approached by Özyörük and Long (1996) using a three-dimensional Euler solver coupled with the Kirchhoff method and by Rumsey *et al* (1998) using a Navier–Stokes indirect solver coupled with the Kirchhoff method.

Although being extensively used in problems involving fluid dynamics, the lattice Boltzmann method has only been explored by a limited number of researchers to specifically predict acoustic wave phenomena. Skordos (1995) simulated the interaction between fluid flow and acoustic field within organ pipes. Buick *et al* (1998) simulated the propagation of linear sound waves using different boundary conditions and latter Buick *et al* (2000) simulated the formation of shock waves. Haydock and Yeomans (2001) predicted the acoustic streaming around a cylinder and between two plates of finite length. More recently, Haydock (2005) also predicted the influence of the fluid viscosity on the force impinged by an acoustic field on a rigid cylinder.

The objective of this paper is to demonstrate that the lattice Boltzmann technique can be used to predict the sound field from a radiating waveguide through the direct solution of the Navier–Stokes equation, representing an alternative to the traditional techniques based on continuum theory. For that, we calculate the normal mode reflection coefficient, end correction and acoustic far field from an unflanged cylinder and compare the results with the solutions presented by Levine and Schwinger.

The next section introduces the lattice Boltzmann technique used in this paper. Section 3 discusses the problem of plane mode acoustic radiation from waveguides, summarizes the exact analytical solutions available and describes the numerical model. Section 4 presents the comparison between analytical solutions and numerical results obtained in terms of end correction, reflection coefficient and directivity factor. Finally, in section 5 we present the conclusions from the results obtained in the previous section.

## 2. Lattice Boltzmann D2Q9 model

Lattice Boltzmann (LB) is classified as a *nonequilibrium* method, whereby the fluid domain is investigated at the particle level. The acoustic field is described by the positions and velocities of all particles within the grid at all time steps. A full description of the lattice Boltzmann

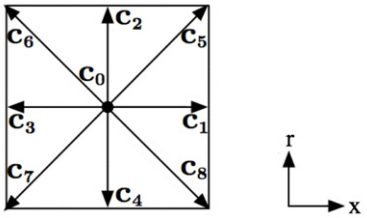


**Figure 1.** The squared grid for the axisymmetric D2Q9 lattice Boltzmann model.

theory can be found in several works (Qian *et al* 1992, He and Luo 1997, Wolf-Gladrow 2000, Succi 2001). LB evolved from the cellular automata method by adopting a simplification of the Boltzmann equation to describe straightforward collision rules that conserve mass and momentum.

In this paper, we use a D2Q9 model first proposed by Qian *et al* (1992) and adapted for pipe flows by Halliday *et al* (2001). The adaptation is based on the assumption that the flow is symmetric about the pipe's axis and thus can be expressed by the incompressible Navier–Stokes equations in cylindrical polar coordinates. Following this assumption, the derivatives associated with the azimuthal coordinate $\vartheta$, as well as the azimuthal component of velocity $u_\vartheta$ vanish, which allows the flow to be simply represented by the axial and radial coordinates, $x$ and $r$, respectively. Hence, the continuum and momentum equations are expressed by

$$\frac{\partial \mathbf{u_x}}{\partial x} + \frac{\partial \mathbf{u_r}}{\partial r} = -\frac{\mathbf{u_r}}{r} \tag{1}$$

$$\frac{D\mathbf{u_x}}{Dt} = -\frac{1}{\rho_0}\frac{\partial p}{\partial x} + \upsilon\nabla^2\mathbf{u_x} + \frac{\upsilon}{r}\frac{\partial \mathbf{u_x}}{\partial r} \tag{2}$$

$$\frac{D\mathbf{u_r}}{Dt} = -\frac{1}{\rho_0}\frac{\partial p}{\partial r} + \upsilon\nabla^2\mathbf{u_r} + \frac{\upsilon}{\mathbf{r}}\left(\frac{\partial \mathbf{u_r}}{\partial \mathbf{r}} - \frac{\mathbf{u_r}}{\mathbf{r}}\right) \tag{3}$$

where $p$ is the pressure, $\upsilon$ is the fluid's kinematic viscosity and $\mathbf{u_x}$ and $\mathbf{u_r}$ are the axial and radial components of the velocity, respectively.

Halliday *et al* (2001) have shown that equations (1)–(3) can be fully recovered from the lattice Boltzmann equation by performing a Chapman–Enskog expansion. However, this is only achievable by inserting space- and time-dependent 'source' terms into the standard lattice Boltzmann equation (see equation (4)).

Identically to the standard D2Q9 model, the adapted version is represented by a two-dimensional squared lattice with nine sites. Each site connects to a neighbour lattice by a unity vector $\mathbf{c}_i$, where $i = 1, 2, \ldots, 8$ indicates the site number, with the exception of the rest site $i = 0$, represented by the null velocity vector $\mathbf{c}_0$ as illustrated in figure 1. The rest site plays an important role in improving the model accuracy by removing the unphysical velocity dependency of pressure (Qian *et al* 1995).

The adapted Boltzmann equation uses the simplified Bhatnagar–Gross–Krook (BGK) collision function approximation defined with a single relaxation time $\tau$, given by

$$f_i(x + c_{ix}, r + c_{ir}, t + 1) - f_i(x, r, t) = -\frac{1}{\tau}\left[f_i(x, r, t) - f_i^M(x, r, t)\right] + h_i' + h_i'' \tag{4}$$

where $f_i$ are the distribution functions associated with the vectors $\mathbf{c}_i$ at a site defined by the axial and radial coordinates $x$ and $r$ and time $t$. $f_i^M$ are the equilibrium distribution functions

which depend on the local fluid velocity $\mathbf{u}(x, r, t)$ and local fluid density $\rho(x, r, t)$. $h_i'$ and $h_i''$ are the inserted source terms so that equations (1)–(3) can be recovered. One should note that the presence of the source terms in equation (4) represents the only distinction from the standard BGK lattice Boltzmann equation.

The general expressions of the equilibrium functions $f_i^M$ associated with the D2Q9 model are given by

$$f_i^M = \begin{cases} \rho w_i \left[1 + 3\mathbf{c}_i \cdot \mathbf{u} + \frac{9}{2}(\mathbf{c}_i \cdot \mathbf{u})^2 - \frac{3}{2}\mathbf{u}^2\right] & \text{for} \quad i = 1, 2, \ldots, 8 \\ \rho\left[\frac{4}{9} - \frac{2}{3}\mathbf{u}^2\right] & \text{for} \quad i = 0 \end{cases} \tag{5}$$

with $w_1 = w_2 = w_3 = w_4 = 1/9$ and $w_5 = w_6 = w_7 = w_8 = 1/36$.

The source terms on the right-hand side of equation (4) are expressed by

$$h_i' = -\frac{w_i \rho_0 u_r}{r} \tag{6}$$

$$h_i'' = w_i \frac{3\upsilon\rho_0}{r}\left[\partial_y \frac{p}{\rho_0} + \partial_x u_x u_r + \partial u_r u_r + c_{ix}(\partial_r u_x - \partial_x u_r)\right]. \tag{7}$$

The stresses and higher order fluxes in equation (7) can either be calculated by means of discrete difference approximations of second-order accuracy or in terms of higher order moments of $f_i$. In our simulation, we use the second approach proposed by Lee *et al* (2005). The derivation of the source terms $h_i'$ and $h_i''$, as well as the techniques for solving equation (7) is described in Halliday *et al* (2001) and Lee *et al* (2005).

The local macroscopic variables $\rho$ and $\mathbf{u}$ are obtained in terms of the moments of the local distribution function $f_i$ by

$$\rho(x, r, t) = \sum_i f_i(x, r, t) \qquad \rho(x, r, t)\mathbf{u}(x, r, t) = \sum_i f_i(x, r, t)\mathbf{c}_i. \tag{8}$$

The left-hand side of equation (4) represents the convection operator and determines the diffusion of the distribution functions $f_i$ over the lattice grid. The right-hand side determines the rate of change of $f_i$ due to intermolecular collisions. This process, known as relaxation, forces $f_i$ towards equilibrium and controls the viscosity of the fluid, recovering its nonlinear form whereby the nonlinear Navier–Stokes equation in cylindrical polar coordinates is satisfied. The Chapman–Enskog expansion on equation (4) (Lee *et al* 2005) gives the expressions for the macroscopic parameters such as pressure $p$, viscosity $\upsilon$ and speed of sound $c_0$ by

$$p = \frac{\rho}{3}, \qquad \upsilon = \frac{2\tau - 1}{6} \qquad \text{and} \qquad c_0 = \frac{1}{\sqrt{3}}. \tag{9}$$

## 3. Radiation from an open unflanged pipe

In this section, we consider the problem of acoustic radiation due to the inviscid propagation of plane waves within an open unflanged cylinder. In this circumstance, when the outgoing wave reaches the open end of the waveguide, part of its energy is returned in terms of a reflected wave with the same modal characteristics. The remainder of the energy is transported away into the external space by a spherical wave. The velocity potential inside the waveguide is the same as if the waveguide were lengthened by a fraction of its open-end radius. The reflection coefficient $R$, defined as the complex ratio between the pressure magnitudes of the reflected and incident waves, the end correction $l$ and the angular distribution of the emitted radiation expressed in terms of directivity factor $G_\phi$ are functions of frequency.

The directivity factor $G_\phi$ is symmetric about a waveguide's axis if the waveguide is also symmetric about the same line. Thus, in the case of a straight cylinder, $G_\phi$ is described by a single angle $\phi(x, r)$ measured from the cylinder's axis at a distance $d$ away from its open end.

Our goal now is to determine the end correction $l$, the amplitude and phase of the reflected wave, represented by the reflection coefficient $R$, and the directivity factor $G_\phi$ from a straight cylinder. We then compare the results with those provided by Levine and Schwinger (1948) for inviscid normal mode propagation. The axisymmetric nature of the problem allows us to use the model described in the previous section to estimate these parameters.

### *3.1. Summary of the exact analytical solution*

The analytical expressions presented below have been obtained for a cylinder with negligible wall thickness by the application of the Wiener–Hopf technique and are correct provided that only dominant mode propagation takes place in the pipe. This requires the value of the maximum frequency of analysis to be inferior to that of the cut-off frequency for dominant modes. In the case of cylinders, the cut-off frequency for dominant modes can be expressed in terms of the characteristic parameter $ka$ and is determined by the first zero of the derivative of a first-order Bessel function of the first type. In this case, $ka = 3.82$.

By choosing the end of the pipe as the reference plane, the complex reflection coefficient in terms of velocity potential for the dominant mode is given by

$$R = \exp\left[\frac{2ka}{\pi}\int_0^{ka}\frac{\tan^{-1}(-J_1(x)/N_1(x))}{x[(ka)^2 - x^2]^{1/2}}\,\mathrm{d}x - 2\mathrm{i}kl\right]. \tag{10}$$

Here and in the following, $J_1$ and $N_1$ are Bessel and Neumann functions of the first order and first type, respectively. The end correction, in units of the pipe radius, is given as

$$\frac{l}{a} = \frac{1}{\pi}\int_0^{ka}\left[\frac{\log[\pi J_1(x)[(J_1(x))^2/N_1(x)]^{1/2}]}{x[(ka)^2 - x^2]^{1/2}}\right]\mathrm{d}x + \frac{1}{\pi}\int_0^{\infty}\left[\frac{\log[1/(2I_1(x)K_1(x))]}{x[x^2 + (ka)^2]^{1/2}}\right]\mathrm{d}x \tag{11}$$

where $I_1$ and $K_1$ are both first-order modified Bessel functions of first and second kinds, respectively.

The normalized far-field directivity factor obtained by the Winer–Hopf technique is given by

$$G_\phi = 2\left(\frac{2ka}{\pi}\right)^{1/2}\frac{J_1(ka\sin\phi)}{\sin\phi(1+\cos\phi)^{1/2}}\frac{|R|}{1-|R|^2} \times \exp\left[ka\cos\phi - \frac{1}{\pi}\int_0^{\infty}\frac{\tan^{-1}(K_1(x)/\pi I_1(x))}{(x^2+(ka)^2)^{1/2} + ka\cos\phi}\frac{x\,\mathrm{d}x}{(x^2+(ka)^2)^{1/2}}\right]. \tag{12}$$

The integrals in equations (10)–(12) are evaluated numerically using the adaptive Lobatto quadrature method. The infinity upper limits found on the integrals of equations (11) and (12) are truncated at a value equal to 100, although the integrals converge for upper limits much smaller than this.

### *3.2. Numerical simulation*

Our computational model is represented by a closed-open cylinder inserted in a fluid domain surrounded by open boundaries as illustrated in figure 2. The square grid is defined with 1000 lattices along each axis. The walls of the cylinder, as well as its closed end, are represented

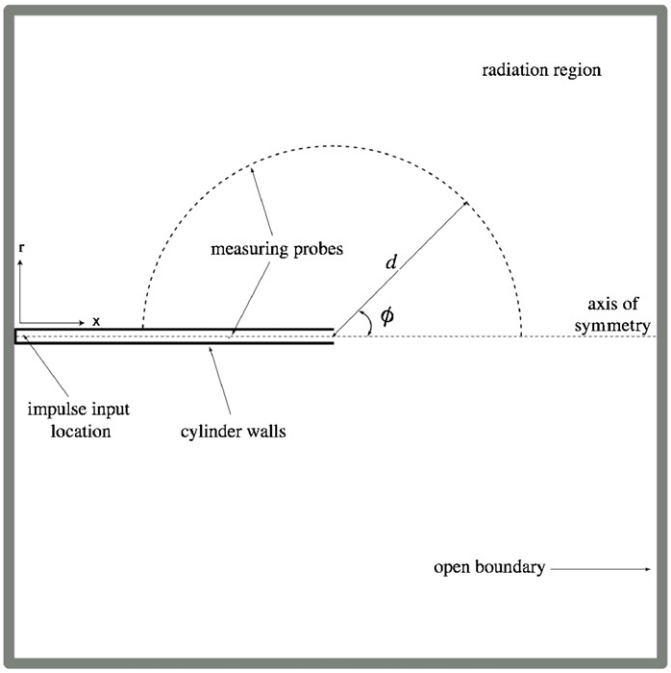


**Figure 2.** Scheme of the axisymmetric lattice Boltzmann model of a radiating unflanged pipe.

with dry lattices of thickness $\delta = 1$. The cylinder has the length $L = 500$ and radius $a = 10$. Here and in the following, the dimensions are expressed in terms of lattice cells.

In order to validate our lattice Boltzmann model based on the analytical solutions presented in the previous section, two restrictions must be taken into account. First, the solutions are only valid for inviscid wave propagation. Secondly, the wall thickness of the cylinder is assumed to be infinitely small. We circumvent the problem associated with the first restriction by choosing a specular free-slip boundary condition (Succi 2001) to avoid transfer of momentum by the tangential motion of particles along the walls and thus force the effect of acoustic boundary layer to be negligible. Furthermore, we choose the viscosity $\upsilon = 9.5 \times 10^{-4}$ which corresponds to a trade-off between a negligible viscosity and the smallest value supported by the BGK scheme before being affected by numerical instabilities[1]. The second restriction is overcome by adopting the modified version of equation (12) for cylinders with finite wall thickness, as proposed by Ando (1968). In this case, the value of $a$ is replaced by the value of the outer radius $a_o$, so that $a_o = a + \delta$.

As a matter of convenience, we use an undisturbed fluid density $\rho_0 = 1$. A density perturbation $\rho' = 0.001$ was applied at the closed end of the cylinder in order to excite the system from its rest state (see figure 2). The perturbation was implemented in the form of a Hanning impulse, so that $\rho = \rho_0 + \rho'\left[0.5 + 0.5\cos\left(\frac{2\pi x}{N} + \pi\right)\right]$ and $\mathbf{u}_x = \frac{\rho' c_0}{\rho_0}\left[0.5 + 0.5\cos\left(\frac{2\pi x}{N} + \pi\right)\right]$, where $N = 10$ was the width of the impulse. The use of a smooth impulse is necessary to minimize the production of high-frequency noise associated with the BGK scheme, as previously mentioned. The magnitude of the impulse is chosen

[1] The effect of the numerical instabilities associated with small viscosities in the BGK scheme is evidenced in terms of high-frequency noise caused by the use of a single relaxation time $\tau$ for the entire set of discrete velocities representing the collision function in equation (4), as described in Lallemand and Luo (2000).

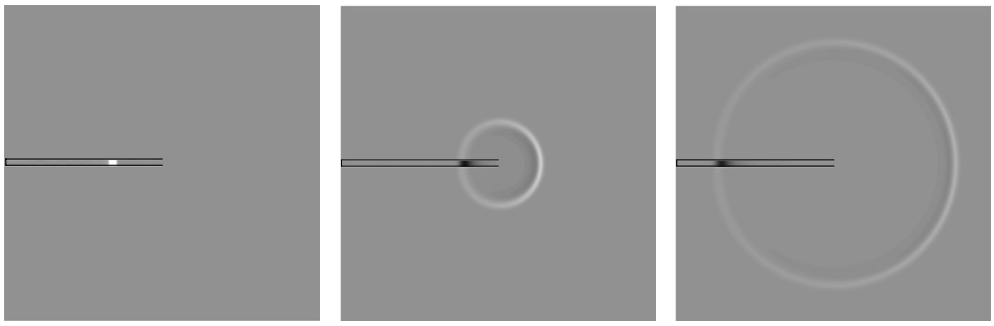

(*a*) (*b*) (*c*)

**Figure 3.** Snapshots from the LB simulation of the radiating cylinder. The figures represent the propagation and radiation of the input perturbation in terms of pressure for different time steps: (*a*) $t = 600$, (*b*) $t = 1093$ and (*c*) $t = 1537$.

to be sufficiently small to guarantee linear wave propagation. We expect the disturbance to propagate as a wavefront throughout the cylinder until the open end where it will be partially reflected and partially radiated to the outer domain in terms of spherical waves with axisymmetric characteristics. Figures 3(*a*)–(*c*) depict different time steps of the lattice Boltzmann simulation.

## 4. Results

### *4.1. Reflection coefficient and end correction*

The complex reflection coefficient for plane waves at any point $x$ inside the cylinder is given by

$$R(x,\omega) = Z_0\left(\frac{Z(x,\omega)/Z_0 - 1}{Z(x,\omega)/Z_0 + 1}\right) \tag{13}$$

where $\omega$ is the angular frequency, $Z(x,\omega)$ is the acoustic impedance, defined as the ratio between the acoustic pressure $P(x,\omega)$ and the volume velocity $\mathbf{U}_x(x,\omega)$, and $Z_0$ is the characteristic impedance of a cylinder. When the acoustic dissipation is negligible, $Z_0$ is a constant given by $\rho_0 c_0/A$, where $A$ is the cylinder's cross-section area.

$P(x,\omega)$ and $\mathbf{U}_x(x,\omega)$ are obtained by performing a discrete Fourier transform (DFT) of the time histories associated with the lattice pressure $p(x,t)$ and the lattice velocity $\mathbf{u}_x(x,t)$ after the system has been excited by the input perturbation at time $t = 0$. However, $p$ and $\mathbf{u}_x$ cannot be directly measured at the end of the pipe due to the fact that the wavefront becomes distorted as it approaches the output, and thus equation (13) is no longer valid. In order to guarantee a plane wavefront, the values of $p$ and $\mathbf{u}_x$ are measured inside the pipe at $x = -\Delta$ before the pipe opening, where $\Delta > 2a_o$. Dalmont *et al* (2001) present an expression for the determination of the complex reflection coefficient $R_{\text{end}}(\omega)$ at the end of the cylinder based on the acoustic impedance $Z_\Delta(\omega)$ measured inside the cylinder at a distance $-\Delta$ from its open end, given by

$$R_{\text{end}}(\omega) = \frac{\mathrm{j}\tan[\arctan(Z_\Delta(\omega)/\mathrm{j}Z_0) - k\Delta] - 1}{\mathrm{j}\tan[\arctan(Z_\Delta(\omega)/\mathrm{j}Z_0) - k\Delta] - 1}. \tag{14}$$

In order to correctly evaluate $R_{\text{end}}$, the impedance $Z_\Delta$ is determined from the values of $p$ and $\mathbf{u}_x$ representing the time history of one round trip of the input perturbation from the measuring

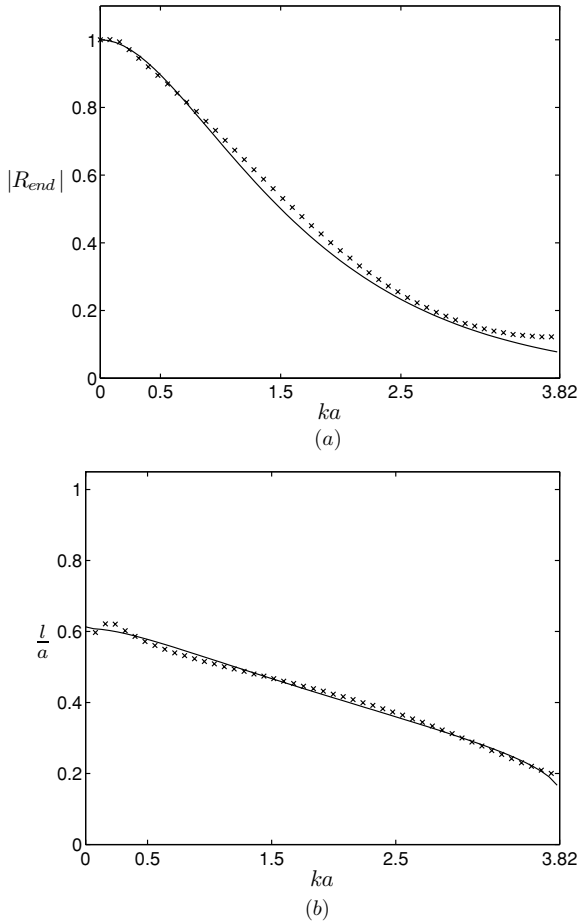


**Figure 4.** Comparison between analytical and numerical results. The solid lines represent the analytical results and crosses represent numerical results. ($a$) Magnitude value of the complex reflection coefficient at the end of the cylinder as a function of the characteristic parameter $ka$. ($b$) End correction $l$ in terms of cylinder radius $a$ as a function of the characteristic parameter $ka$.

point inside the cylinder to its open end. The end correction $l$ is associated with the phase of $R_{\text{end}}$ and is given Pierce (1981):

$$l = \frac{1}{2jk} \ln\left(\frac{R_{\text{end}}}{|R_{\text{end}}|}\right). \tag{15}$$

Figures 4($a$) and ($b$) depict the comparisons between theory and numerical results for the magnitude of the reflection coefficient $|R_{\text{end}}|$ and the end correction, $l$, as functions of the characteristic parameter $ka$.

The general trend found on the numerical result of the magnitude of the reflection function, $R_{\text{end}}$, shows that the fraction of reflected energy at the open end is usually higher than the one predicted by the theory (figure 4($a$)). The highest discrepancy between theoretical and numerical results is seen at the region around $ka = 1.5$ where numerical values are higher by $\sim$8%. A better agreement is found in the comparison of results related to the end correction, $l$ (figure 4($b$)). In this case, the highest disagreement is found in the low-frequency region (small values of $ka$) where the numerical result is $\sim$4% higher than the analytical prediction.

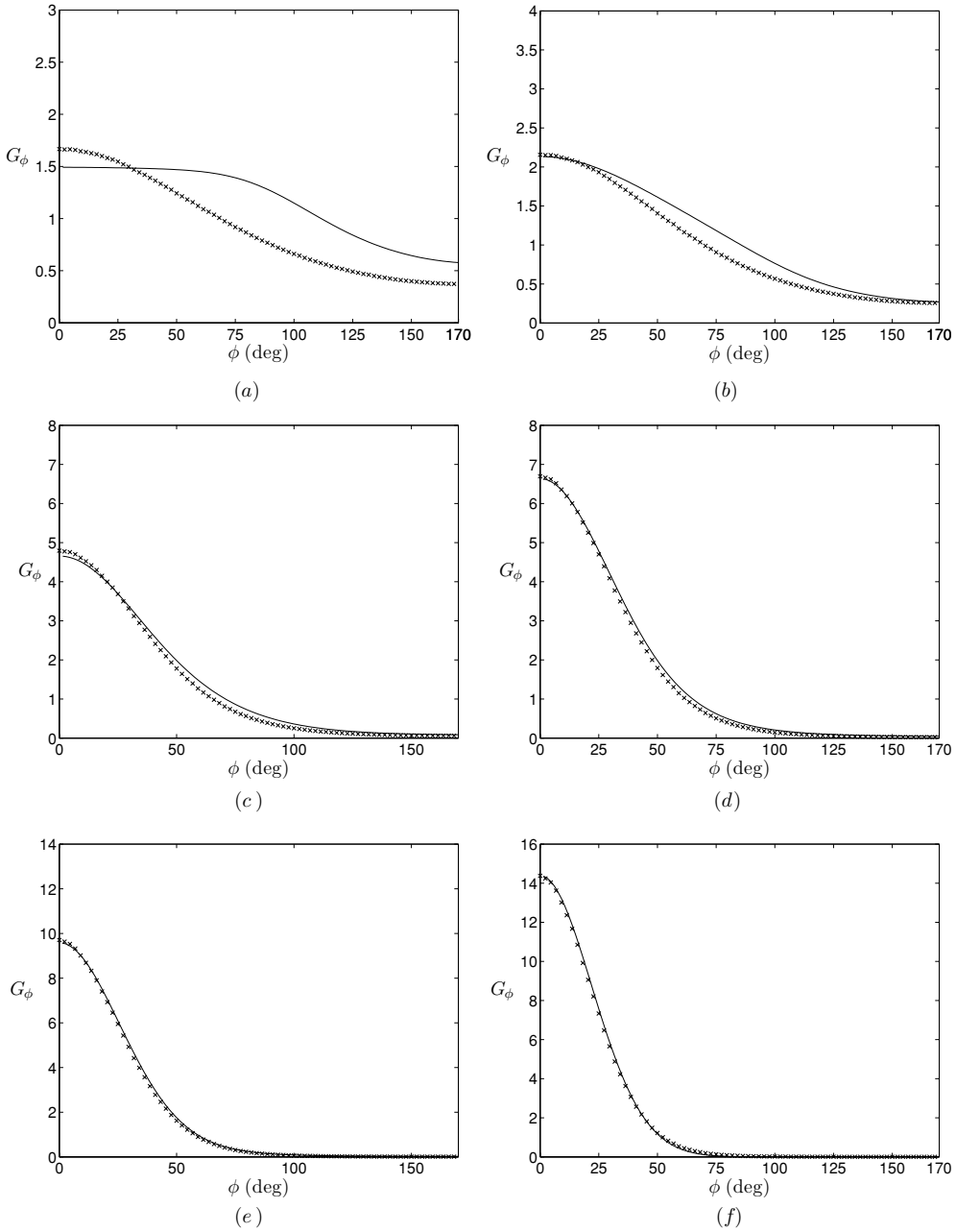


**Figure 5.** Directivity factor $G_\phi$ as a function of the angle $\phi$ measured from the axis of the cylinder for different values of $ka$. The crossed points represent the numerical results and the solid line represents the analytical: (*a*) $ka = 0.48$, (*b*) $ka = 1.0$, (*c*) $ka = 2.0$, (*d*) $ka = 2.50$, (*e*) $ka = 3.0$ and (*f*) $ka = 3.77$.

The discordance between results was expected and is likely to be due to energy leakage caused by the truncation of the time history associated with $p$ and $\mathbf{u}_x$ prior to the application of the discrete Fourier transform to derive $Z_\Delta$ in equation (14). The truncation acts as if the

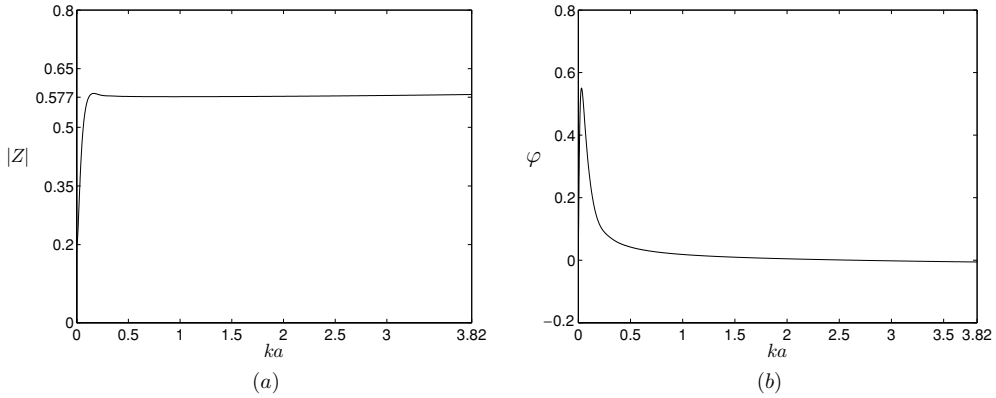


**Figure 6.** Evaluation of the region of $ka$ at which the far-field condition is satisfied for a distance $r = 250$ and $\phi = 0^\circ$: (*a*) radiation impedance and (*b*) phase between acoustic pressure and particle velocity.

resulting spectra of $p$ and $\mathbf{u}_x$ were obtained by the convolution in frequency of their non-truncated spectra with the spectrum of a rectangular window having the same duration as $p$ and $\mathbf{u}_x$ and magnitude equal to the unity (Oppenheim and Shafer 1999). We could minimize the effect of truncation by increasing the size of the time histories of $p$ and $\mathbf{u}_x$. However, the open boundary in the model (see figure 2) is not perfectly anechoic. Therefore, reflections from that region would return back to the measuring points and, consequently, compromise the simulation

### *4.2. Radiation directivity*

We now present the results obtained for the radiation directivity $G_\phi$, measured from the axis of the pipe. The definition of $G_\phi$ is given by

$$G_\phi = \frac{P_\phi^2}{P_h^2} \tag{16}$$

where $P_\phi^2$ is the mean-square sound pressure at angle $\phi$ and distance $d$ from a directional acoustic source of a certain acoustic power, whereas $P_h^2$ is the mean-square sound pressure from an omnidirectional source of equal acoustic power, measured at the same distance.

In our simulation we evaluate $P_\phi$ by performing a DFT on the values of $p_\phi$ measured at 85 different angles from the axis of the cylinder between $\phi = 0^\circ$ and $\phi = 170^\circ$. For economy reasons, we restricted our analysis to a fixed distance $d = 250$ from the cylinder's open end. $P_h$ is evaluated from the averaged value of $P_\phi^2$ along the angles.

Figure 5 presents the results for the directivity factor $G_\phi$. A poor agreement between analytical and numerical results can be seen for small values of $ka$, particularly when $ka < 1$, as depicted in figures 5(*a*) and (*b*). Conversely, the agreement increases as $ka \to 3.82$. This trend is explained by the fact that $G_\phi$ can only be measured in a far-field region whose minimum distance is inversely proportional to the frequency of the acoustic source. The far-field condition is satisfied when the acoustic impedance $Z$ of the diverging spherical wave approximates that of a plane wave, i.e., $Z \to \rho_0 c_0$ and $\varphi \to 0$, where $\varphi$ is the phase between acoustic pressure and particle velocity.

Figure 6 presents the plots of $Z$ and $\varphi$ as functions of $ka$, obtained from the LB model at a distance $d = 250$ and angle $\phi = 0$. They illustrate the values of $ka$ from which the far-field condition can be assumed and explain the discrepancy between theoretical and numerical results for the directivity factor $G_\phi$, particularly for values of $ka < 1$, as shown in figure 5.

The graphics depicted in figure 6 show that, although the impedance $Z$ converges rapidly to $\rho_0 c_0$[2] for small values of $ka$ (figure 6($a$)), the phase between acoustic pressure and particle velocity, $\varphi$, only approximates zero for values of $ka > 2$ (figure 6($b$)).

## 5. Conclusions

In this paper, we demonstrated that a BGK lattice Boltzmann model can be used to accurately predict the acoustic far field of a radiating cylinder when considering normal mode radiation. We also used this technique to predict the other variables associated with the radiation process, namely, the effective length of the cylinder and the reflection coefficient at the open end, both as functions of the characteristic parameter $ka$.

In general, the results of the simulation agreed well with the analytical solution proposed by Levine and Schwinger for inviscid wave propagation. They also suggested that a large fluid domain is required for the prediction of the directivity factor $G_\phi$, as well as for the prediction of the parameters associated with the reflection at the open end, namely $R_{\text{end}}$ and $l$. In the first case, the large domain is necessary for the fulfilment of the far-field condition at low frequencies. In the second case, a large domain is desired to enlarge the time histories of the particle velocity $\mathbf{u}_x$ and acoustic pressure $p$ in order to minimize the effect of truncation.

In future, we plan to investigate the influence of the acoustic viscous layer on the directivity pattern and, added to that, the influence of the interaction between acoustic and fluid fields when a turbulent flow is present. Another substantial direction is to consider radiation due to higher propagation modes such as transversal spinning modes.

## Acknowledgment

The first author would like to thank CAPES (Funding Council of the Brazilian Ministry of Education) for supporting his research.

## References

Ando Y 1968 *Acustica* **20** 366–9
Buick J M, Buckley C L, Greated C A and Gilbert J 2000 *J. Phys. A: Math. Gen.* **33** 3917–28
Buick J M, Greated C A and Campbell D M 1998 *Europhys. Lett.* **43** 235–40
Chen X X, Zhang X, Morfey C L and Nelson P A 2004 *J. Sound Vib.* **270** 573–86
Dalmont J P, Nederveen C J and Joly N 2001 *J. Sound Vib.* **244** 505–34
Halliday I, Hammond L A, Care C M, Good K and Stevens A 2001 *Phys. Rev.* E **64** 011208
Haydock D 2005 *J. Phys. A: Math. Gen.* **38** 3265–77
Haydock D and Yeomans J M 2001 *J. Phys. A: Math. Gen.* **34** 5201–13
He X and Luo L S 1997 *Phys. Rev.* E **56** 6811–7
Howe M S 1984 *J. Appl. Math.* **32** 187–209
King L V 1936 *Phil. Mag.* **21** 128–44
Lallemand P and Luo L S 2000 *Phys. Rev.* E **61** 6546–62
Lee T S, Huang H and Shu C 2005 *Int. J. Mech. Fluids* **49** 99–116
Levine H and Schwinger J 1948 *Phys. Rev.* **73** 383–406
Oppenheim A V and Shafer R W 1999 *Discrete-Time Signal Processing* 2nd edn (Englewood Cliffs, NJ: Prentice-Hall)

[2] $\rho_0 = 1$ and $c_0 = 1/\sqrt{3}$.

Özyörük Y and Long L 1996 *Am. Inst. Aeronaut. Astronaut. J.* **34** 894–901
Pierce A D 1981 *Acoustics: An Introduction to its Physical Principles and Applications* (*McGraw-Hill Series in Mechanical Engineering*) (New York: McGraw-Hill)
Powell A 1964 *J. Acoust. Soc. Am.* **36** 177–95
Qian Y, d'Humires D and Lallemand P 1992 *Europhys. Lett.* **17** 479–84
Qian Y, Succi S and Orszag S A 1995 *Annu. Rev. Comp. Phys.* **3** 195–242
Rayleigh J W S 1877 *Theory of Sound* vol 2, 1 edn (New York: Dover)
Rumsey C L, Biedron R T and Farassat F 1998 *J. Sound Vib.* **213** 643–64
Schlichting H 2004 *Boundary Layer Theory* 8th edn (Berlin: Springer)
Skordos P A 1995 Modeling flue organ pipes: sub-sonic flow, lattice Boltzmann, and parallel distributed computers *PhD Thesis* Massachusetts Institute of Technology
Succi S 2001 *The Lattice Boltzmann Equation for Fluid Dynamics and Beyond* (Oxford: Oxford University Press)
Tyler J M and Sofrin T G 1962 *SAE Transact.* **70** 309–32
Williams J E F and Hawkings D L 1969 *Phil. Trans. R. Soc. London* **264** 321–42
Wolf-Gladrow D A 2000 *Lattice Gas Cellular Automata and Lattice Boltzmann Models: An Introduction* (*Lecture Notes in Mathematics*) (Berlin: Springer)